nature communications

Article

https://doi.org/10.1038/s41467-024-52788-3

A reversible photochromic covalent organic framework

Received: 19 April 2024

Accepted: 23 September 2024

Published online: 01 October 2024

Check for updates

Xue-Tian Li[1], Meng-Jing Li[1], Yuan-Liang Tian[1], Shu-Lin Han[2], Lei Cai[2], Hui-Chao Ma[1], Ying-Qiang Zhao[1], Gong-Jun Chen[1] ✉ & Yu-Bin Dong[1] ✉

Covalent organic frameworks are a type of crystalline porous materials that linked through covalent bond, and they have numerous potential applications in adsorption, separation, catalysis, and more. However, there are rarely relevant reported on photochromism. Fortunately, a hydrazone-linked DBTB-DETH-COF is rapidly generated through ultrasound method. The DBTB-DETH-COF is found to exhibit reversible photochromism (at least 50 cycles) from yellow to olive in the presence of light and air, and subsequently back to the original color upon heating. In addition, the structure of DBTB-DETH-COF remains unchanged after 15 days of light illumination. Furthermore, the reason of photochromic process is discussed by electron paramagnetic resonance, X-ray photoelectron spectroscopy, electrochemistry characterizations and transient absorption measurements. The reversible photochromic DBTB-DETH-COF can be used as anti-counterfeiting ink and optical switch in the presence of air. This work expands a stable organic photochromic material and broadens the applications of COFs.

In the past decade, there was a lot of attention given to photochromic materials that respond to color changes in the light stimulus and usually reversible[1–5], owing to their attractive applications include switching, logic gates, anticounterfeiting, information storage, optoelectronic devices, environmental monitoring, superior bioimaging, and so forth[6–14]. Nowadays, a number of inorganic, organic and inorganic-organic hybrid photochromic materials have been explored[5,15–17]. The common inorganic photochromic materials include polyoxometalates, transition metal oxides, metal halides, prussian blue analogs and rare earth complexes, etc. The classic organic photochromic materials contain dithienylethene, spiropyrans, diarylethenes, chromenes, fulgides, azocompounds, viologens, and so on. The inorganic-organic hybrid photochromic materials cover hybrids of metal halides, hybrids of metal cyanides, hybrids of polyoxometalates, metal chalcogenide, and metal-organic complexes, etc. The photochromism are mainly due to the change oxidation states upon irradiation, photo-induced molecular conformations isomerization, polarity, and photoinduced electron transfer[18–22]. Design and synthesis of stable photochromic materials featuring fast response and high contrast are still a challenging task[23,24]. As a recently emerging class of porous crystalline materials assembled through strong covalent bonds, covalent organic frameworks (COFs) have become attractive platforms for various functional materials, including gas adsorption and storage, energy storage and conversion, drug delivery, and heterogeneous catalysis owing to their unique features including permanent porosity, low densities, and high surface areas. These advantages enable COFs to readily adsorb guest molecules and establish interactions with them. The more important thing is COFs have relatively high chemical, light and thermal stabilities, which make them more suitable for practical applications[25–28]. Photochromic COFs through reversible trans-cis isomerization or ring-closing/opening have been developed[29,30]. However, there is no report other type photochromic COF. Herein, we display a DBTB-DETH-COF which exhibits reversible photochromism owing to photoinduced electron transfer (PET) in the

[1]College of Chemistry, Chemical Engineering and Materials Science, Collaborative Innovation Center of Functionalized Probes for Chemical Imaging in Universities of Shandong, Key Laboratory of Molecular and Nano Probes, Ministry of Education, Shandong Normal University, Jinan 250014, P. R. China. [2]Shandong Province Key Laboratory of Medical Physics and Image Processing Technology, School of Physics and Electronics, Shandong Normal University, Jinan 250014, P. R. China. ✉e-mail: gongjchen@126.com; yubindong@sdnu.edu.cn

presence of light and oxygen. What's more important is the photochromism and restoration process can be repeated at least 50 cycles without color loss. This work not only develops a stable organic photochromic material, but also expands the application of COFs materials as anti-counterfeiting ink and optical switch.

Results and discussion

Synthesis and structure of DBTB-DETH-COF

More than 10 g crystalline DBTB-DETH-COF was quickly obtained within 1 h from the condensation of 4,4′-dihydroxy-[1,1′-biphenyl]−3,3′,5,5′-tetracarbaldehyde (DBTB) and 2,5-diethoxyterephthalohydrazide (DETH) under ultrasound conditions as shown in Fig. 1. The as-synthesized DBTB-DETH-COF was characterized by Fourier-transform infrared spectroscopy (FT-IR). The emerging stretching vibration peak at 1620 cm^{-1} was observed, confirming the formation of a C = N linkage (Supplementary Fig. 1a)[31]. The solid-state cross-polarization with magic angle spinning (CP/MAS) ^{13}C NMR spectrum exhibited a resonance signal at 150.2 ppm, corresponding to the chemical shift of imine carbon atoms in DBTB-DETH-COF (Supplementary Fig. 1b)[32]. These results confirm the successful synthesis of DBTB-DETH-COF by the condensation reaction. The structure of DBTB-DETH-COF was analyzed by powder X-ray diffraction (PXRD) experiment and theoretical simulation using the Materials Studio (ver. 2018). As shown in Fig. 2a, four dominant diffraction peaks appear at 4.44°, 6.30°, 8.98°and 26.5°, which can be assigned to the (1 0 0), (1 $\bar{1}$ 0), (0 2 0) and (0 0 1) reflections. To interpret the lattice information, the calculation was adopted to optimize the conformation of the 2D eclipsed (AA) stacking model. In contrast, their staggered (AB) model did not agree with the experimental results (Supplementary Fig. 1c). The PXRD pattern with the P_1 space group gave the unit cell parameters of $a = b = 20.4000$ Å, $c = 3.4200$ Å, and $\alpha = \beta = 90°$, $\gamma = 84.1964°$. The reproducible parameters are in line with the experimentally observed pattern with a negligible difference (Rwp = 2.09% and Rp = 1.56%). The thermal stability of the DBTB-DETH-COF was estimated by thermal gravimetric analysis (TGA) under a nitrogen atmosphere. As shown in Supplementary Fig. 1d, DBTB-DETH-COF was thermally stable to 360 °C. The N_2 adsorption−desorption experiment at 77 K exhibits a type I isotherm feature (Supplementary Fig. 1e). The Brunauer-Emmett-Teller (BET) surface area is calculated as 357.4 m^2/g. The pore diameters calculated by the NLDFT algorithm was 1.4 nm, which is very close to the theoretical value of 1.6 nm. Scanning electron microscopy (SEM) images of DBTB-DETH-COF revealed fiber morphology (Supplementary Fig. 1f). HR-TEM revealed that DBTB-DETH-COF has grid structure with pores of around 1.5 nm (Fig. 2b), which is well consistent with its structural modeling analysis. In order to optimize the synthesis conditions of DBTB-DETH-COF, the control experiments were conducted as the water temperature was raised to 60 °C under ultrasound condition. The experiments under ultrasound at 0 °C for 1 h and heating at 60 °C for 1 h did not obtain high crystalline DBTB-DETH-COF (Supplementary Fig. 2). But DBTB-DETH-COF with high crystalline can be obtained under solvothermal conditions in the dioxane/mesitylene mixture was sealed in a Pyrex tube at 120 °C for 3 days (Supplementary Fig. 3). The ultrasonic method is more efficient and time saving, more importantly, it is easier to obtain a large amount of products compared to traditional solvothermal approach. The stability of DBTB-DTPH-COF formed through solvothermal method and the ultrasound method are also similar (Supplementary Fig. 4). It is noteworthy that DBTB-DTPH-COF has poor stability in NaOH solution.

Photochromic transformation of DBTB-DETH-COF

DBTB-DETH-COF exhibits a promising photochromic transformation from yellow to olive upon exposure to xenon light for 5 min (Fig. 3, Supplementary Movie 1). The olive sample can be decolored after being heated at 100 °C for 5 min (Supplementary Movie 2). The DBTB-DETH-COF obtained under solvothermal condition exhibit the same photochromic behavior as the DBTB-DETH-COF obtained under ultrasound (Supplementary Fig. 5). However, there are no photochromic features under light or air alone, and no photochromic phenomenon was observed under nitrogen or carbon dioxide atmosphere when illuminated. But under oxygen conditions, photochromism occurs when illuminated, and the original color of DBTB-DETH-COF recovery under heating conditions (Supplementary Fig. 6). In addition, the comparative experiments with DBTB and monomer model N′-(2-Hydroxybenzylidene)benzohydrazide (Supplementary Fig. 7, Supplementary Table 1 and Table 2) and N′,N″,N‴,N⁗-((1E,1′E,1″E,1‴E)-(4,4′-dihydroxy-[1,1′- biphenyl]−3,3′,5,5′- tetrayl) tetrakis (methanylidene)) tetra (benzohydrazide) (Supplementary Fig. 7, Supplementary Fig. 8) are made under the same conditions, the photochromic behavior cannot be observed. Furthermore, the photochromic process has been further investigated by solid-state UV−vis spectroscopy. As depicted a new electron absorption band with peak ranging from 500 to 800 nm appear after photochromism (Fig. 3a). Before photochromism of DBTB-DETH-COF (BP-DBTB-DETH-COF) and after photochromism of DBTB-DETH-COF (AP-DBTB-DETH-COF) display yellow and olive respectively, because they absorb their complementary light. The optical bandgap energies (Eg) of BP-DBTB-DETH-COF and AP-DBTB-DETH-COF based on Tauc plots were estimated to be 2.58 and 1.76 eV, respectively (Fig. 3b)[33], this result indicates that the DBTB-DETH-COF possessed a semiconductor feature and after photochromism bandgap energies reduce. The narrower band gap of AP-DBTB-DETH-COF

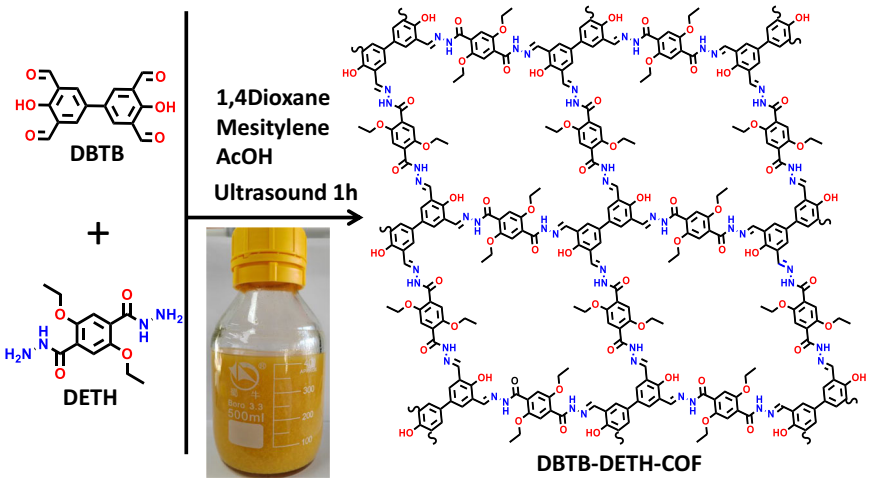

Fig. 1 | Synthesis and structure. The schematic diagram for synthesis and structure of DBTB-DETH-COF.

https://doi.org/10.1038/s41467-024-52788-3

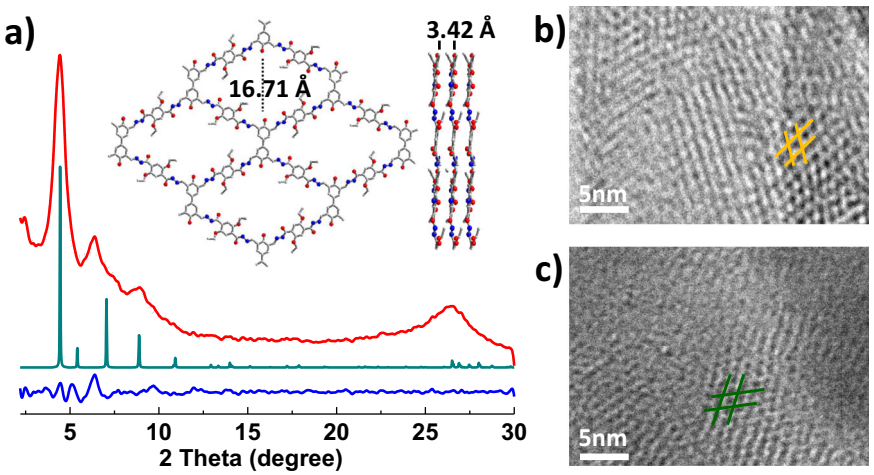

Fig. 2 | The structure characterization and analysis of DBTB-DETH-COF. a PXRD patterns of DBTB- DETH-COF: comparison between the experimental (red line) and Pawley refined (black dots) profiles, the simulated patterns for eclipsed (AA) stacking mode (malachite green line) and the refinement differences (blue line). Insets show the structures of DBTB-DETH-COF. **b** the TEM of DBTB-DETH-COF before photochromism. **c** the TEM of DBTB-DETH-COF after photochromism.

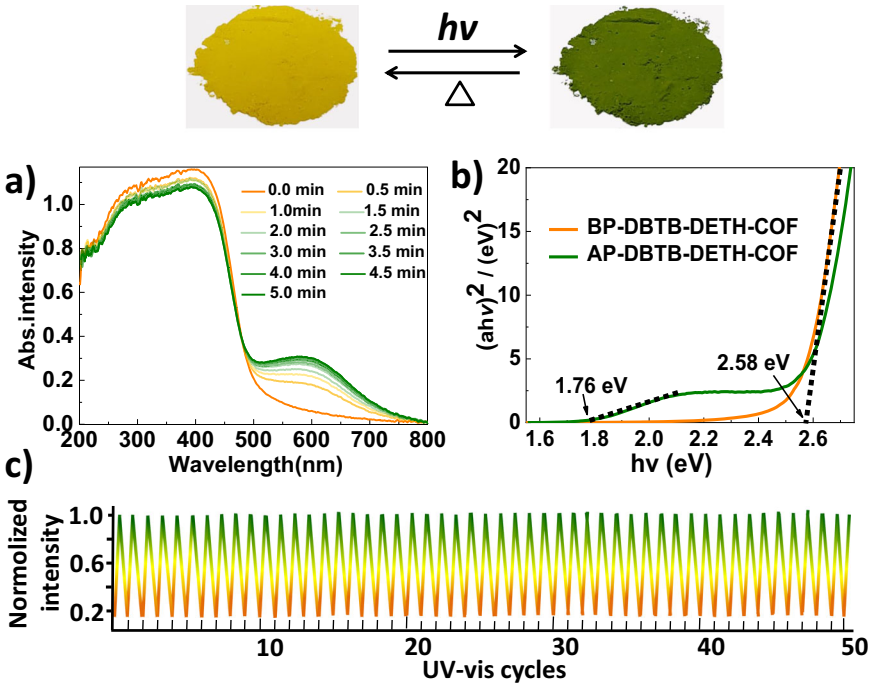

Fig. 3 | Reversible photochromic transformation. a Time-dependent UV−vis diffuse reflectance spectra of DBTB-DETH-COF. **b** Tauc plots of BP-DBTB-DETH-COF and AP-DBTB-DETH-COF. **c** photochromic transformation cycles.

makes it easier to be excited by visible light with lower energy. The process of coloring and bleaching can be completely repeated at least 50 times without any remarkable decrease in color contrast (Fig. 3c), which suggests that DBTB-DETH-COF has high quality reversible photochromic property. In addition, DBTB-DETH-COF is stable except for color changes under light for 15 days, which was verified by the measured TEM profiles (Fig. 2c), PXRD, FT-IR, BET, TGA, and SEM (Supplementary Fig. 9). AP-DBTB-DETH-COF is essentially identical with BP-DBTB-DETH-COF, suggesting that DBTB-DETH-COF has strong fatigue-resistance property and no bond cleavage/formation or lattice rearrangement occurs. DBTB-DETH-COF did not exhibit photochromic phenomenon under illumination in the absence of oxygen, indicating that DBTB-DETH-COF itself does not exhibit photochromic behavior.

Electron paramagnetic resonance of DBTB-DETH-COF

Electron paramagnetic resonance (EPR) spectroscopy is a powerful tool to judge which species is generated in the photochromic system. For the solid sample, DBTB-DETH-COF has the ESR signal before and after photoirradiation, and the intensity of signals increased after photochromism (Fig. 4a). It was easily inferred that more free charge carriers could be generated in DBTB-DETH-COF under light irradiation. To further confirm the reactive oxygen species (ROS), the ESR spectroscopy was conducted using corresponding spin trapping agents in the presence of DBTB-DETH-COF. 2,2,6,6-tetramethylpiperidine (TEMP) in acetonitrile as the singlet oxygen ($^1O_2$) trapping agent and 5, 5-Dimethyl-pyridine-N-oxide (DMPO) in methanol as the superoxide anions ($\bullet O_2^-$) trapping agent and DMPO in water as hydroxyl radical ($\bullet$OH) trapping agents, respectively[34]. As depicted in Fig. 4b, the

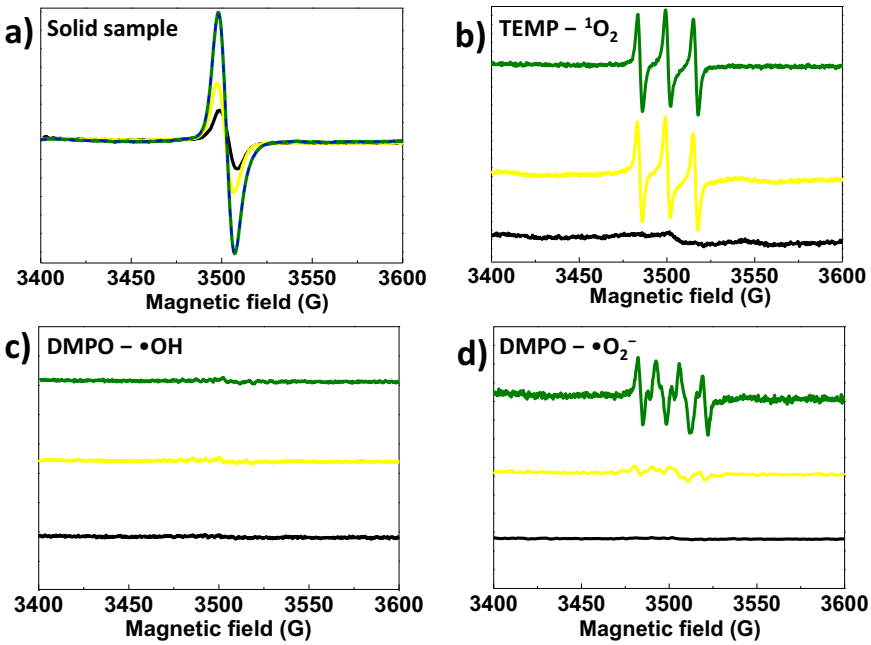

Fig. 4 | ESR spectra. a ESR spectra of solid DBTB-DETH-COF before irradiation and after irradiation. **b** ESR of DBTB-DETH-COF in the presence of TEMP. **c** ESR of DBTB-DETH-COF in water with the presence of DMPO. **d** ESR of DBTB-DETH-COF in methanol with the presence of DMPO. (the black line represents the DBTB-DETH-COF in the dark. The orange line represents that the DBTB-DETH- COF remains yellow after being illuminated for 1 min. The olive line represents the sample displays olive color illuminated for 5 min).

intensity of three characteristic peaks of $^1O_2$ after photochromism are equal to the intensity of before photochromism, which indicate that the formation of $^1O_2$ had nothing to do with photochromism. Moreover, the EPR signal of the DMPO − •OH adduct was not observed before and after photochromism (Fig. 4c), which confirm that photochromism has a negligible effect on •OH generation. The characteristic peaks of $•O_2^-$ does not appear for in dark, and the peaks intensity after photochromism increases significantly compared to that before photochromism (Fig. 4d), which confirm that photochromism of DBTB-DETH-COF is trigged the generation of superoxide radicals in the presence of oxygen and light. In addition, to further confirm the photochromic mechanism, a series of controlled experiments were carried out using $AgNO_3$ as an electron scavenger, KI as a hole scavenger, benzoquinone as $•O_2^-$ scavenger, isopropanol as •OH scavenger and NaN_3 as $^1O_2$ scavenger[35]. The yellow BP-DBTB-DETH-COF sample in different scavenger under light irradiation, only in benzoquinone has no color variation (Supplementary Fig. 10a). The different quenching agents were added to the olive sample (AP-DBTB-DETH-COF), benzoquinone can formed yellow formazan (Supplementary Fig. 10b), which further confirm that photochromism of DBTB-DETH-COF is due to the formation of $•O_2^-$.

X-ray photoelectron spectroscopy of DBTB-DETH-COF

To gain a deeper insight into the effect of the valence state changes before and after photochromism, X-ray photoelectron spectroscopy (XPS) tests were performed. The C1s spectrum before and after photochromism displayed three peaks at 288.4 eV (C = O), 285.7 eV (C = N/C-O) and 284.8 eV (C − C/C = C), respectively[36]. The N1s spectrum of BP-DBTB-DETH-COF and AP-DBTB-DETH-COF showed two peaks at 400.4, and 399.5 eV, which were assigned to C = N and C-N, respectively. There is no significant change for the valence states of C1s and N1s before and after photochromism. The O1s binding energy peaks of BP-DBTB-DETH-COF are located at 531.3 eV and 533.1 eV, which corresponded to C-OH/C-O-C and C = O, while after photochromism the O1s spectra can be fitted two peaks :531.5 eV and 532.2 eV, respectively (Fig. 5)[37–39]. The shift of both peaks towards higher binding energy indicates a decrease in the electron cloud density of the C-OH/C-O-C and C = O bond, which suggest that the electrons of BP-DBTB-DETH-COF have been transferred to O_2. This is in good agreement with the EPR experiment. The full XPS spectra is displayed in Supplementary Fig. 11a, b and XPS valence band spectra of DBTB-DETH-COF before and after photochromism are 2.50 and 1.75 V, respectively (Supplementary Fig. 11c, d)[40].

Electrochemical testing of DBTB-DETH-COF

In order to clarify the energy band of DBTB-DETH-COF before and after photochromism, Mott−Schottky experiment were then performed (Fig. 6a)[41,42], the positive slopes of the Mott-Schottky plots suggest that DBTB-DETH-COF is an n-type semiconductor, the conduction band (CB) position of BP-DBTB-DETH-COF was fitted to be −0.73 eV vs SCE (corresponding to −0.53 eV vs NHE), which is more negative than the CB position of AP-DBTB-DETH-COF (−0.34 eV vs NHE), and flat-band potential of BP-DBTB-DETH-COF is negative enough for the reduction of O_2 to $•O_2^-$ (−0.33 eV)[43]. Based on the values of optical bandgap and conduction band potential, the valence band potential was estimated to be 2.05 and 1.42 eV (Fig. 6b). AP-DBTB-DETH-COF has a lower band gap. The charge transfer properties of DBTB-DETH-COF are measured by electrochemical impedance spectroscopy (EIS) and photocurrent response. AP-DBTB-DETH-COF shows the smaller semicircle (Fig. 6c), suggesting its lower interfacial charge transfer resistance. The photocurrent intensity of AP-DBTB-DETH-COF is significantly higher than that of BP-DBTB-DETH-COF under the same conditions (Fig. 6d)[44]. This also proves that the photochromism behavior is mainly originated from oxygen reacts with DBTB-DETH-COF to form superoxide anions, and the increases of free charge carriers in the system result the higher charge migration rate.

Transient absorption of DBTB-DETH-COF

For the sake of getting detailed information about the excited state of DBTB-DETH-COF under light irradiation, the transient absorption (TA) spectroscopy measurements were performed (Fig. 7). The TA spectra of DBTB-DETH-COF under nitrogen and oxygen atmosphere show negative features at 440 nm due to ground state bleaching process,

https://doi.org/10.1038/s41467-024-52788-3

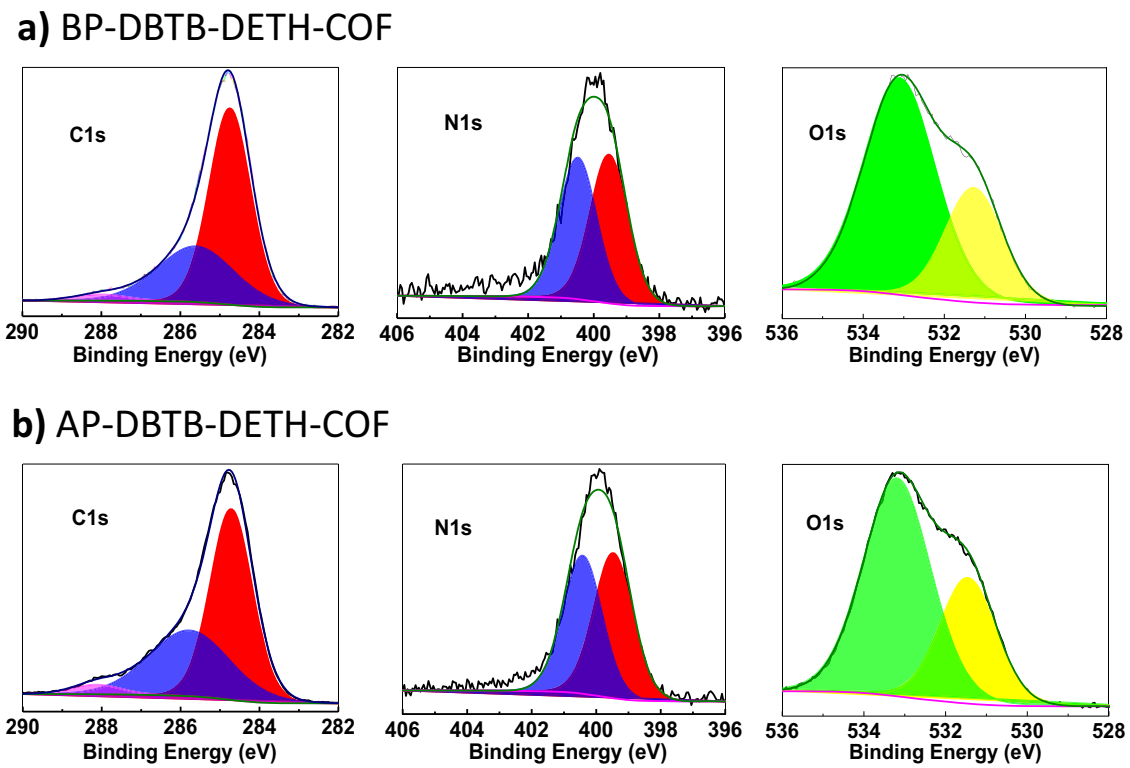

Fig. 5 | XPS spectra. a BP-DBTB-DETH-COF. **b** AP-DBTB-DETH-COF.

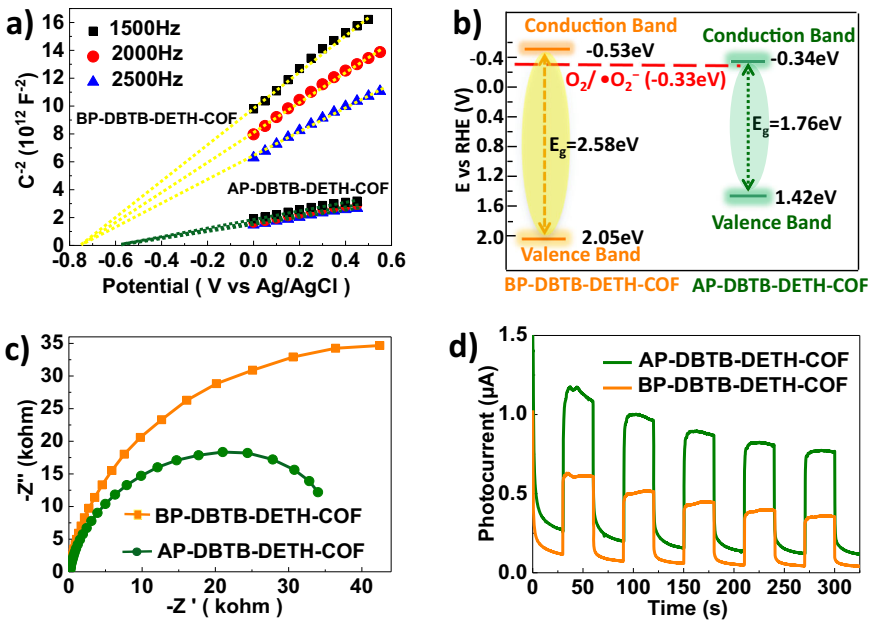

Fig. 6 | Electrochemical characteristics of DBTB-DETH-COF. a Mott–Schottky plots of BP- DBTB-DETH-COF and AP-DBTB-DETH-COF. **b** Band structures of BP-DBTB-DETH-COF and AP-DBTB-DETH-COF. **c** EIS Nyquist plots of BP-DBTB-DETH-COF and AP-DBTB-DETH-COF. **d** Photocurrent responses of BP-DBTB-DETH-COF and AP-DBTB-DETH-COF.

which also corresponds to the steady state absorption spectra of DBTB-DETH-COF (Fig. 3a)[45]. Both conditions display the maximum positive value at 575 nm, this signal can be assigned to the absorption derived from PET and the signal value in oxygen is greater than that in nitrogen, which suggesting that oxygen can promote electron transfer. No photochromism occurred under light without O_2, indicating photochromism is not caused by electron transfer within BP-DBTB-DETH-COF itself, but due to photoinduced electron transfer (PET) between DBTB-DETH-COF and O_2. Photochromism of DBTB-DETH-COF occurs under oxygen and light, the presence of $•O_2^-$ was detected through EPR, indicating that DBTB-DETH-COF reacted with O_2 to produce $•O_2^-$, and the transfer of electrons from BP-DBTB-DETH-COF to O_2 was confirmed by XPS and TA. BP-DBTB-DETH-COF undergoes a color change to form AP-DBTB-DETH-COF after losing electrons, while O_2

https://doi.org/10.1038/s41467-024-52788-3

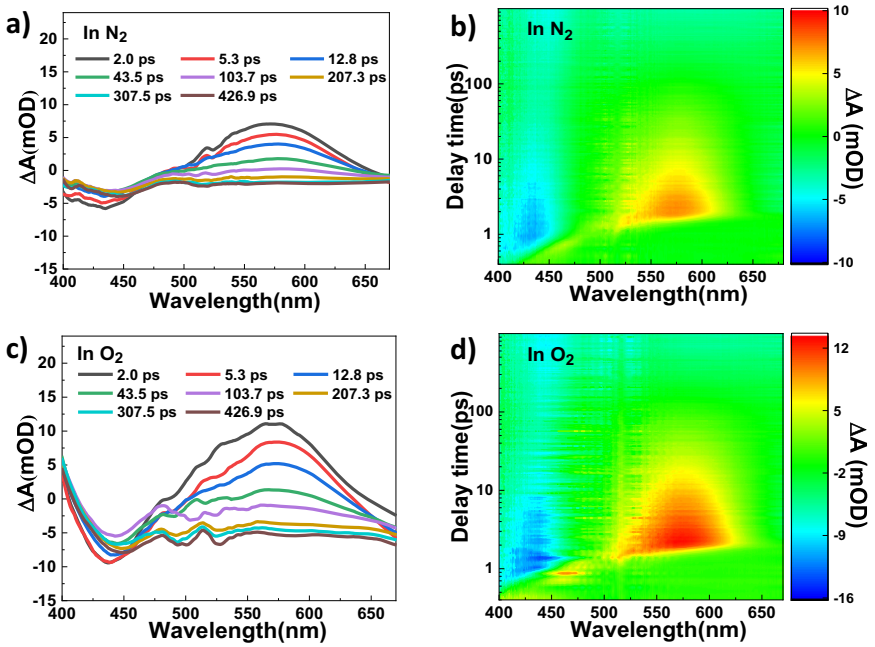

Fig. 7 | Transient absorption spectra of DBTB-DETH-COF. a DBTB-DETH-COF under N_2 atmosphere. **b** two-dimensional spectro-temporal transient absorption map showing the change in optical density (OD) in N_2. **c** DBTB-DETH-COF under O_2 atmosphere. **d** two-dimensional spectro- temporal transient absorption map showing the change in optical density (OD) in O_2 (343 nm excitation).

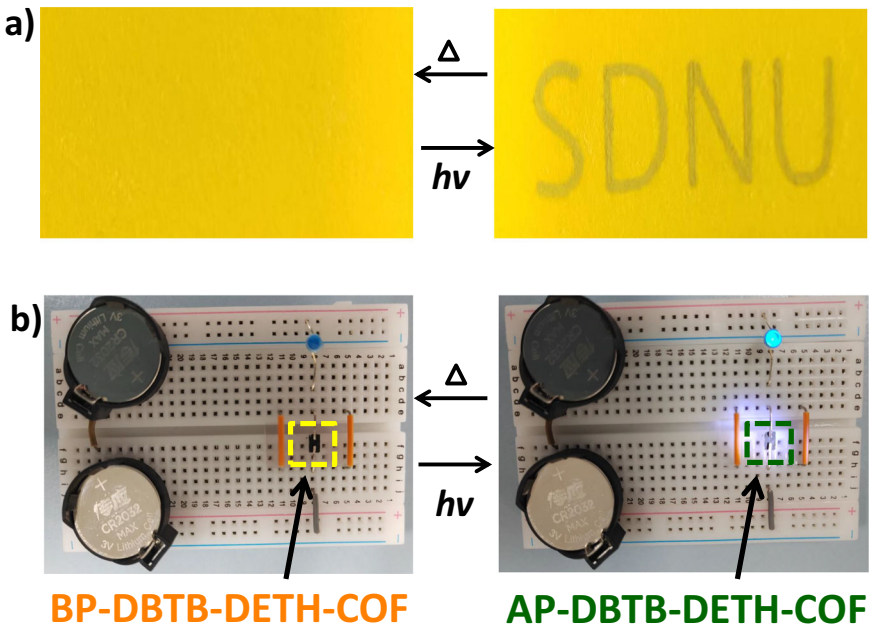

Fig. 8 | The usage of DBTB-DETH-COF. a Application in anticounterfeiting. **b** The photoswitch device of DBTB-DETH-COF.

form $\bullet O_2^-$ after gaining electrons. Additionally, the pore structure of DBTB-DETH-COF plays a role in stabilizes the $\bullet O_2^-$. Under heating conditions, $\bullet O_2^-$ return electrons to AP-DBTB-DETH-COF form O_2 and BP-DBTB-DETH-COF, the COF restore the original color.

Utilized in anti-counterfeiting ink and light switch

Owing to the highly stable reversible photochromic properties, the obtained DBTB-DETH-COF can potentially be used as an anti-counterfeiting ink[46]. As demonstrated in Fig. 8a, The DBTB-DETH-COF dispersed in ethanol and used this yellow solution to write letters on yellow paper, the letters were invisible. Subsequently, the words became visible to naked eyes as olive color after the paper was exposed to light. The letters are invisible again after heating. The olive color characters reappear under light. These experiments demonstrated DBTB-DETH-COF have the potential application for anti-counterfeiting ink. The reversible on-off could be repeated for >50 cycles without significant loss in contrast. To further demonstrate the DBTB-DETH-COF has more practical application. The difference in optoelectronic performance before and after photochromism encourage us to explore for DBTB-DETH-COF as a light switch[30]. The

conductivity of DBTB-DETH-COF is too low to make the LED lamp turns on. After doping graphene in DBTB-DETH-COF (Supplementary Fig. 12), the LED lamp turns on in light and air, and turns off after heating (Fig. 8b). Graphene/DBTB-DETH-COF can act as a light switch when air is present and this photoswitch device can also be seen as chemical sensor of O_2. The reversible on–off could be repeated for >30 cycles.

In summary, a photochromic system DBTB-DETH-COF has been developed and characterized. It displays high-contrast naked-eye distinguished color changes from yellow to olive after exposure to light and DBTB-DETH-COF retains its original structure after 15 days of illumination. Through comprehensive experimental of XPS, EPR, electrochemistry characterizations and TA, it is disclosed that the reversible photochromic properties of DBTB-DETH-COF could be attributed to the electron transfer from DBTB-DETH-COF to oxygen to generate superoxide anions, the photochromism of DBTB-DETH-COF cause changes in the energy band and conductivity. Therefore, DBTB-DETH-COF can detect oxygen in light using LED lamp. This work will provide a strategy to obtain photochromic COF with anti-counterfeiting application and oxygen molecular recognition.

Methods

Materials

Biphenyl-4,4′-diol (98.0 %), Diethyl-2,5-dihydroxyterephthalate (98.0 %), Iodoethane (99 %), Salicylaldehyde (99.0 %), Benzoyl hydrazine (98.0 %), Acetic acid (99.5 %), Potassium carbonate (99.0 %) and Anhydrous trifluoroacetic acid (TFA, 99.5 %) were purchased from Macklin Biochemical Co., Ltd. 1,4-Dioxane (99 %), Mesitylene (99.0 %), Ethanol (99.7 %), Methanol (99.5 %), N,N-Dimethylformamide (DMF, 99.5 %), Dichloromethane (99.8%), Acetonitrile (99.7 %) and Dimethyl sulfoxide (DMSO, 99.8 %) were purchased from Tianjin Fuyu Fine chemical Co., Ltd. Toluene (98.0 %), Hydrazine hydrate (80.0 %), Hexamethylenetetramine (98.0 %), HCl (36.0 ~ 38.0 %), NaOH (98.0 %) and $NaBH_4$ (98.0 %) were purchased from Sinopharm Chemical Reagent Co., Ltd. Nafion solution (5 %) was purchased from Sigma-Aldrich. The reagents and solvents employed were commercially available and used without further purification.

Synthesis of DBTB-DETH-COF

The DBTB-DETH-COF prepared by ultrasound with the monomers of DBTB (135 mmol, 3.55 g) and DETH (265 mmol, 7.50 g) in the dioxane/mesitylene (200.0 / 200.0 mL). After stirring for 2 min, acetic acid (6 M, 50.0 mL) was added, and the above solution was kept under ultrasound conditions (200 W, 80 kHz) for 1 h. After that, the resultant yellow precipitate denoted as DBTB-DETH-COF was filtered and washed with DMF, dichloromethane and ethanol, and finally dried in vacuum at 80 °C overnight (93 % yield).

The photochromic procedure for DBTB-DETH-COF

BP-DBTB-DETH-COF exhibits a promising photochromic transformation from yellow to olive after irradiation with visible-light under xenon lamp (300 W with the intensities 2.5 W cm^{-2}) for 5 min. And the sample AP-DBTB-DETH-COF is heated on heating plate at 100 °C for 5 min. The olive sample restore to yellow.

EPR characterization

Powder sample (5 mg) of DBTB-DETH-COF was separately added to nuclear magnetic tubes. The main frequency is 9.550 GHz. The scan range is 200 G, from 3400 G to 3600 G. The sealed tube was then irradiated with a 300 W xenon lamp for 5 min, followed by the same EPR studies. Spin trapping studies for $\bullet O_2^-$ detection: 2 mg of DBTB-DETH-COF was suspended in 95 μL of methanol, followed by the addition of 5 μL of DMPO and irradiated for 5 min. Spin trapping studies for •OH detection: The experiments were performed followed the same procedures as for •OH detection except that 95 μL of H_2O was used instead of 95 μL of methanol. Spin trapping studies for $^1O_2$ detection: The experiments were performed followed the same procedures as for $\bullet O_2^-$ detection except that 5 μL of TEMP was used instead of 5 μL DMPO and 95 μL of acetonitrile was used instead of 95 μL of methanol.

Mott-Schottky plots and electrochemical impedance spectroscopy (EIS)

EIS were carried out with a CHI 660E electrochemical workstation using a three-electrode system. Typically, 4 mg DBTB-DETH-COF, 1 mL mixed solution of isopropyl alcohol and H_2O (volume ratio of 1 – 3) and 30 μL Nafion mixed solution were mixed together, and 5 μL mixture was coated on the glassy carbon as working electrodes. The Na_2SO_4 solution (0.1 mol L^{-1}) was utilized as the electrolyte. The Mott-Schottky plot was recorded with frequencies of 1500, 2000, and 2500 Hz, respectively.

Photocurrent measurements

Photocurrent measurements were carried out with a CHI 660E electrochemical workstation (ShangHai ChenHua, China) using a three-electrode system. Typically, 4 mg DBTB-DETH-COF, 1 mL mixed solution of isopropyl alcohol and H_2O (volume ratio of 1 – 3) and 30 μL Nafion mixed solution were mixed together, and 200 μL mixture was coated on the FTO glass as the working electrodes. The Pt plate was utilized as the counter electrode (CE) and the Ag/AgCl as a reference electrode (RE). A 300 W Xenon lamp equipped with the cut-off filter was used as the light source. The Na_2SO_4 solution (0.1 mol L^{-1}) was utilized as the electrolyte. The photocurrent signals were recorded with a bias potential of +0.5 V.

Transient absorption measurements

The 1030 nm output pulse from the fiber laser was split in two parts with a beam splitter, one is used to pump beam, which accounts for 70%, another one is used to probe beam, which accounts for 30%. The 343 nm pulses were achieved by partially pumping two BBO crystals through the transmitted part. Use a 2 kHz synchronous chopper to chop the pump pulse. The reflected 1030 nm pulses first pumped a BBO crystal to generate a second harmonic, and then focuses on sapphire to produce ultraviolet-white beam (400 nm–700 nm). The delay time between the pump and probe pulsed was controlled by a motorized delay stage. The probe beam was focused with an Al parabolic reflector onto the sample. The probe beam was received by a fiber-coupled spectrometer at a frequency of 4 kHz. The samples were placed in 1 mm airtight cuvettes in air and measured under ambient conditions.

Anticounterfeiting ink DBTB-DETH-COF

1 mg of DBTB-DETH-COF is thoroughly ground into a uniform powder in the mortar, 0.5 mL ethanol is added, the mixture is ultrasonic for 5 min, and then the sample is evenly coated on the yellow matrix with glass capillary tubes to form the desired shape, and finally dried at 80 °C.

The photoswitch device of DBTB-DETH-COF

DBTB (0.135 mmol, 35.5 g), DETH (0.265 mmol, 75 mg) and graphene (7 mg) in the dioxane/mesitylene (20.0 / 20.0 mL). After stirring for 2 min, acetic acid (6 M, 5.0 mL) was added, and the above solution was kept under ultrasound conditions (200 W, 80 kHz) at room temperature for 1 h. After that, the resultant black precipitate denoted as graphene /DBTB-DETH-COF was filtered and washed with DMF, dichloromethane and ethanol, and finally dried in vacuum at 80 °C overnight, and then the graphene /DBTB-DETH-COF is pressed into sheets under a tablet press. After cutting the rectangular sample, it can be used for photoswitch. Finally, connect the switching device, electronic light bulb, and power supply device into a circuit to form an photoswitch circuit device.

Data availability

Source data are present with this paper that supports the findings of this study. Crystallographic data for the structures reported in this Article have been deposited at the Cambridge Crystallographic Data Centre, under deposition numbers CCDC: 2373149 (N′-(2-Hydroxybenzylidene)benzohydrazide). The data can be obtained free of charge via https://www.ccdc.cam.ac.uk/structures. Source data are provided with this paper.

References

1. Exelby, R. & Grinter, R. Phototropy (or photochromism). *Chem. Rev.* **65**, 247–260 (1965).
2. Jia, S., Ye, H., He, P., Lin, X. & You, L. Selection of isomerization pathways of multistep photoswitches by chalcogen bonding. *Nat. Commun.* **14**, 7139 (2023).
3. Fihey, A., Perrier, A., Browne, W. R. & Jacquemin, D. Multi-photochromic molecular systems. *Chem. Soc. Rev.* **44**, 3719–3759 (2015).
4. Wang, L. & Li, Q. Photochromism into nanosystems: towards lighting up the future nanoworld. *Chem. Soc. Rev.* **47**, 1044–1097 (2018).
5. Jago, D., Gaschk, E. E. & Koutsantonis, G. A. History and fundamentals of molecular photochromism. *Aust. J. Chem.* **76**, 635–654 (2023).
6. Irie, M., Fukaminato, T., Matsuda, K. & Kobatake, S. Photochromism of diarylethene molecules and crystals: memories, switches, and actuators. *Chem. Rev.* **114**, 12174–12277 (2014).
7. Wang, S., Fan, W., Liu, Z., Yu, A. & Jiang, X. Advances on tungsten oxide based photochromic materials: strategies to improve their photochromic properties. *J. Mater. Chem. C.* **6**, 191–212 (2018).
8. Li, Z. et al. Photoresponsive luminescent polymeric hydrogels for reversible information encryption and decryption. *Adv. Sci.* **6**, 1901529 (2019).
9. Andréasson, J. & Pischel, U. Light-stimulated molecular and supramolecular systems for information processing and beyond. *Coord. Chem. Rew.* **429**, 213695 (2021).
10. Wang, Y., Zhang, Y.-M. & Zhang, S. X.-A. Stimuli-induced reversible proton transfer for stimuli-responsive materials and devices. *Acc. Chem. Res.* **54**, 2216–2226 (2021).
11. Walden, S. L. et al. Visible light-induced switching of soft matter materials properties based on thioindigo photoswitches. *Nat. Commun.* **14**, 8298 (2023).
12. Zhao, J.-L. et al. Photochromic crystalline hybrid materials with switchable properties: recent advances and potential applications. *Coord. Chem. Rew.* **475**, 214918 (2023).
13. Li, Q.-F. et al. Photochromic diarylethene induced fluorescence switching materials constructed by non-covalent interactions. *J. Mater. Chem. C.* **11**, 12828–12847 (2023).
14. Chatterjee, S., Molla, S., Ahmed, J. & Bandyopadhyay, S. Light-driven modulation of electrical conductance with photochromic switches: bridging photochemistry with optoelectronics. *Chem. Commun.* **59**, 12685–12698 (2023).
15. He, T. & Yao, J. Photochromic materials based on tungsten oxide. *J. Mater. Chem.* **17**, 4547–4557 (2007).
16. Wang, M.-S., Xu, G., Zhang, Z.-J. & Guo, G.-C. Inorganic–organic hybrid photochromic materials. *Chem. Commun.* **46**, 361–376 (2010).
17. Rice, A. M. et al. Photophysics modulation in photoswitchable metal –organic frameworks. *Chem. Rev.* **120**, 8790–8813 (2020).
18. Blfgér, D. & Hecht, S. Visible-light-activated molecular switches. *Angew. Chem. Int. Ed.* **54**, 11338–11349 (2015).
19. Meng, Y.-S., Sato, O. & Liu, T. Manipulating metal-to-metal charge transfer for materials with switchable functionality. *Angew. Chem. Int. Ed.* **57**, 12216–12226 (2018).
20. Wang, J.-X., Li, C. & Tian, H. Energy manipulation and metal-assisted photochromism in photochromic metal complex. *Coord. Chem. Rev.* **427**, 213579 (2021).
21. Han, S.-D., Hu, J.-X. & Wang, G.-M. Recent advances in crystalline hybrid photochromic materials driven by electron transfer. *Coord. Chem. Rev.* **452**, 214304 (2022).
22. Kobayashi, Y. & Abe, J. Recent advances in low-power-threshold nonlinear photochromic materials. *Chem. Soc. Rev.* **51**, 2397–2415 (2022).
23. Kulyk, O., Rocard, L., Maggini, L. & Bonifazi, D. Synthetic strategies tailoring colours in multichromophoric organic nanostructures. *Chem. Soc. Rev.* **49**, 8400–8424 (2020).
24. Thaggard, G. C. et al. Metal–photoswitch friendship: from photochromic complexes to functional materials. *J. Am. Chem. Soc.* **144**, 23249–23263 (2022).
25. Ding, S.-Y. & Wang, W. Covalent organic frameworks (COFs): from design to applications. *Chem. Soc. Rev.* **42**, 548–568 (2013).
26. Waller, P. J., Gándara, F. & Yaghi, O. M. Chemistry of covalent organic frameworks. *Acc. Chem. Res.* **48**, 3053–3063 (2015).
27. Geng, K. et al. Covalent organic frameworks: design, synthesis, and functions. *Chem. Rev.* **120**, 8814–8933 (2020).
28. Yan, D., Wang, Z. & Zhang, Z. Stimuli-responsive crystalline smart materials: from rational design and fabrication to applications. *Acc. Chem. Res.* **55**, 1047–1058 (2022).
29. Das, G. et al. Azobenzene-equipped covalent organic framework: light-operated reservoir. *J. Am. Chem. Soc.* **141**, 19078–19087 (2019).
30. Yu, F. et al. Photostimulus-responsive large-area two-dimensional covalent organic framework films. *Angew. Chem. Int. Ed.* **58**, 16101–16104 (2019).
31. Uribe-Romo, F. J., Doonan, C. J., Furukawa, H., Oisaki, K. & Yaghi, O. M. Crystalline covalent organic frameworks with hydrazone linkages. *J. Am. Chem. Soc.* **133**, 11478–11481 (2011).
32. Stegbauer, L., Schwinghammer, K. & Lotsch, B. V. A hydrazone-based covalent organic framework for photocatalytic hydrogen production. *Chem. Sci.* **5**, 2789–2793 (2014).
33. Huang, W., He, Q., Hu, Y. & Li, Y. Molecular heterostructures of covalent triazine frameworks for enhanced photocatalytic hydrogen production. *Angew. Chem. Int. Ed.* **58**, 8676–8680 (2019).
34. Liu, X. et al. Triazine–porphyrin-based hyperconjugated covalent organic framework for high-performance photocatalysis. *J. Am. Chem. Soc.* **144**, 23396–23404 (2022).
35. Li, Q. et al. Structural and morphological engineering of benzothiadiazole- based covalent organic frameworks for visible light-driven oxidative coupling of amines. *ACS Appl. Mater. Interfaces* **13**, 39291–39303 (2021).
36. Yang, Y.-X. et al. G. Transformation of a hydrazone-linked covalent organic framework into a highly stable hydrazide-linked one. *ACS Appl. Polym. Mater.* **4**, 4624–4631 (2022).
37. Grissa, R. et al. Thermomechanical polymer binder reactivity with positive active materials for Li metal polymer and Li-Ion batteries: An XPS and XPS imaging study. *ACS Appl. Mater. Interfaces* **11**, 18368–18376 (2019).
38. Xu, J. et al. Constructing La2B2O7 (B = Ti, Zr, Ce) Compounds with three typical crystalline phases for the oxidative coupling of methane: the effect of phase structures, superoxide anions, and alkalinity on the reactivity. *ACS Catal.* **9**, 4030–4045 (2019).
39. Guo, X. et al. Fabrication of photoresponsive crystalline artificial muscles based on PEGylated covalent organic framework membranes. *ACS Cent. Sci.* **6**, 787–794 (2020).
40. Ehsan, M. F. et al. $CoFe_2O_4$ decorated g-C_3N_4 nanosheets: new insights into superoxide anion mediated photomineralization of methylene Blue. *J. Environ. Chem. Eng.* **8**, 104556 (2020).

41. Wei, S. et al. Semiconducting 2D triazine-cored covalent organic frameworks with unsubstituted olefin linkages. *J. Am. Chem. Soc.* **141**, 14272–14279 (2019).
42. Ding, J. et al. Three-dimensional covalent organic frameworks with ultra-large pores for highly efficient photocatalysis. *J. Am. Chem. Soc.* **145**, 3248–3254 (2023).
43. Sun, L. et al. Double-shelled hollow rods assembled from nitrogen/sulfur-codoped carbon coated indium oxide nanoparticles as excellent photocatalysts. *Nat. Commun.* **10**, 2270 (2019).
44. Dong, P. et al. Postsynthetic annulation of three-dimensional covalent organic frameworks for boosting CO_2 photoreduction. *J. Am. Chem. Soc.* **145**, 15473–15481 (2023).
45. Cheng, Y. Z. et al. Persistent radical cation sp^2 carbon-covalent organic framework for photocatalytic oxidative organic transformations. *Appl. Catal. B Environ.* **306**, 121110 (2022).
46. Huang, G. et al. Multiple anti-counterfeiting guarantees from a simple tetraphenylethylene derivative-high-contrasted and multi-state mechanochromism and photochromism. *Angew. Chem. Int. Ed.* **58**, 17814–17819 (2019).

Acknowledgements

We gratefully acknowledge the NSFC (Grants Nos. 22371172, Y.B.D.; 22205132, H. C. M.; and 22197153, Y.B.D.), Shandong Provincial Natural Science Foundation (No. ZR2021MB019, G.J.C. and ZR2022QB001, H. C. M.), the Major Basic Research Projects of Shandong Natural Science Foundation (No. ZR2020ZD32, Y.B.D.), and the Taishan Scholars Climbing Program of Shandong Province (Y.B.D.).

Author contributions

All authors contributed extensively to the work presented in this paper. Y.B.D. and G.J.C. conceived the research project. X. T. L., M. J. L., Y. L. T. and H. C. M. conducted the experiments and performed the characterizations. S. L. H. and L. C conducted transient absorption measurements. Y Q. Z. conducted the experiments of XPS. Y.B.D. and G.J.C. wrote the manuscript with the input from the other authors.

Competing interests

The authors declare no competing interests.

Additional information

Supplementary information The online version contains supplementary material available at https://doi.org/10.1038/s41467-024-52788-3.

Correspondence and requests for materials should be addressed to Gong-Jun Chen or Yu-Bin Dong.

Peer review information *Nature Communications* thanks Dong Wang, and the other, anonymous, reviewer(s) for their contribution to the peer review of this work. A peer review file is available.